Macroscopic quantum tunneling of ferromagnetic domain walls

Hans-Benjamin Braun
Paul Scherrer Institut, CH-5232 Villigen PSI, Switzerland

Jordan Kyriakidis and Daniel Loss
Department of Physics and Astronomy, University of Basel, Klingelbergstrasse 82, 4056 Basel, Switzerland
(Received 25 April 1997)

Quantum tunneling of domain walls out of an impurity potential in a mesoscopic ferromagnetic sample is investigated. Using improved expressions for the domain-wall mass and for the pinning potential, we find that the crossover temperature between thermal activation and quantum tunneling is of a different functional form than found previously. In materials such as Ni or yttrium iron garnet, the crossover temperatures are around 5 mK. We also find that the WKB exponent is typically two orders of magnitude larger than current estimates. The sources for these discrepancies are discussed, and precise estimates for the transition from three-dimensional-to-one-dimensional magnetic behavior of a wire are given. The crossover temperatures from thermal-to-quantum transitions and tunneling rates are calculated for various materials and sample sizes. [S0163-1829(97)02638-6]

I. INTRODUCTION

The possibility of observing quantum mechanical behavior at a mesoscopic scale has recently attracted much experimental and theoretical interest. First, there is the fundamental issue of identifying physical systems possessing many degrees of freedom which support a collective mode that features typical quantum properties such as superposition behavior, interference effects, or tunneling through potential barriers. Well-known examples of such systems are Josephson junctions which have been extensively studied in the past (for a review see, e.g., Leggett[1]). Recently the focus has shifted towards low-dimensional magnetic systems[2] such as single-domain ferromagnets and antiferromagnets, but also towards nonuniform magnetic structures exhibiting domain (or Bloch) walls. In the latter case, one envisages a domain wall trapped by a magnetic pinning center—as provided, for example, by an impurity lowering the anisotropy energy locally. The domain wall can then escape from this potential well by tunneling through the energy barrier. The observability of such tunneling events basically depends on three conditions which can be stated qualitatively as follows. First, the tunneling barrier should be neither too high nor too wide. Second, the effective mass associated with the tunneling dynamics of the Bloch wall, and hence the number of spins in the wall, should not be too large. These two conditions are required in order to have a tunneling rate not too small, so that one can expect a tunneling event to take place within a reasonable amount of time (typically on the scale of hours or less). And third, the crossover temperature which separates the classical regime of barrier crossing due to thermal activations from the quantum regime of tunneling should realistically be in the milli-Kelvin range or above. Clearly, a more precise formulation of these conditions is essential since they are of fundamental importance for the interpretation of recent and future experiments in terms of macroscopic quantum tunneling. With this motivation, it is our goal to provide such quantitative estimates in the following.

Although the idea of domain wall tunneling has first been described for bulk samples in the 1970's,[3–5] it was not until the work by Stamp and collaborators[6,7] that this idea has received wider attention. The past few years have seen considerable progress in sample preparation and has made a detailed experimental study of the relaxation properties in nanowires possible.[8] In such experiments, the observation of a temperature independent relaxation (or resistance) below a critical temperature is taken as a strong indication for quantum tunneling. Such observed crossover temperatures lie in the range of 2 to 5 K. Resistivity measurements at low temperatures require metallic samples. The presence of conduction electrons, however, may interfere with the tunneling process by providing a channel for dissipation (although large domain walls or low conductivities reduce this undesirable effect). Insulating samples overcome this problem, but then experiments more difficult than resistance measurements are necessary. Rather than resistivity, magnetization can be measured; a depinned wall which propagates down the sample will be accompanied by a sudden change in the magnetization.

Theoretical estimates, based on the same model considered here, have been given before,[7] but as we shall see the conclusions reached have been too optimistic. In particular, we find the functional dependence of the crossover temperature on experimentally important quantities such as the coercivity and domain wall mass are quite different from earlier calculations. This result has already been stated in Ref. 9, Sec. VII, but without any details given. Below we provide these details, thus supporting earlier claims. The value of the crossover temperature is of considerable interest for the interpretation of experimental observations since it is usually taken as a strong indication for the existence of quantum tunneling if the magnetization switching becomes temperature independent below this crossover temperature. Also, earlier estimates[7] predict reasonable tunneling rates for domain walls containing up to 10^6 spins, whereas we find that the number of spins in a flat wall should not exceed 10^4.
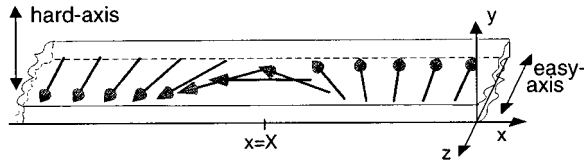
FIG. 1. Shown is a Bloch wall configuration in a thin long slab, i.e., $\theta_0(x-X)$, and $\phi_0 = \pi$.

The paper is organized as follows. In Sec. II we present the model for a ferromagnet. We then discuss the conditions under which transverse spin waves freeze out and the sample can be considered one dimensional. The domain wall mass is derived from the well-known classical soliton solutions, and the origin of the impurity potential is discussed. In Sec. III we evaluate the tunneling rates and crossover temperatures for a domain wall out of a pinning potential. Explicit numerical examples are given for various materials such as yttrium iron garnet (YIG), Ni, and in particular the very promising perovskite and (badly) itinerant ferromagnet $SrRuO_3$.[20,21] These results are summarized in Tables I–III. Finally, we compare these results in Sec. IV with values given previously in Ref. 7.

II. MODEL

We consider an elongated ferromagnetic sample (or "nanowire") as depicted in Fig. 1. We assume that the transverse dimensions w of the sample are small enough to ensure that the system behaves effectively one dimensional (1D) at the typical temperatures T of an experiment. Quantitative estimates for w and T will be given below. Now the energy of an effectively 1D ferromagnet extending along the x axis is given by

$$E[\theta,\phi] = \mathcal{A} \int_{-L/2}^{L/2} dx \{A[(\partial_x\theta)^2 + \sin^2\theta(\partial_x\phi)^2]$$
$$+ K_e \sin^2\theta + K_h \sin^2\theta \, \sin^2\phi\}, \qquad (2.1)$$

where $\mathcal{A}$ is the cross sectional area of the sample and the sample length L is assumed to be much larger than the width of a domain wall. The magnetization has been expressed in polar coordinates, $\mathbf{M} = M_0(\sin\theta\cos\phi, \sin\theta\sin\phi, \cos\theta)$ with $M_0 = g\mu_B s/a^3$ the saturation magnetization and a the lattice constant. The three terms in the energy density of Eq. (2.1) respectively describe isotropic exchange, easy-axis anisotropy (along $\hat{z}$), and hard-axis anisotropy (along $\hat{y}$). The anisotropy terms are of an effective nature and can contain both crystalline and demagnetizing (shape-induced) contributions. A typical example of an elongated sample is shown in Fig. 1 where $K_e = K_{e,\mathrm{cryst}}$ and $K_h = K_{h,\mathrm{cryst}} + 2\pi M_0^2$.[10]

In the absence of dissipation, the dynamics of the magnetization is governed by the familiar Landau-Lifshitz equations

$$\partial_t\phi = -\frac{\gamma}{M_0}\frac{\delta(E/\mathcal{A})}{\delta\cos\theta},$$

$$\partial_t\cos\theta = \frac{\gamma}{M_0}\frac{\delta(E/\mathcal{A})}{\delta\phi}. \qquad (2.2)$$

Here both ϕ and $\cos\theta$ depend on x,t, the energy E is given by Eq. (2.1), and $\gamma = g\mu_B/\hbar$ denotes the gyromagnetic ratio.

A. 1D regime

The system exhibits quasi-1D behavior when all transverse degrees of freedom are frozen out. In order to obtain a quantitative estimate of this 1D regime and thus of the validity of the model (2.1), (2.2), we start from the three-dimensional (3D) spectrum of excitations around a Bloch wall, which is given by[11]

$$\epsilon_{n,\mathbf{k}} = \frac{2a^3}{s}\sqrt{A\mathbf{k}_\perp^2 + n(Ak_x^2 + K_e)}\sqrt{K_h + A\mathbf{k}_\perp^2 + n(Ak_x^2 + K_e)}, \qquad (2.3)$$

and evaluate the corresponding finite size gaps. Here $\mathbf{k}_\perp = (k_y, k_z)$ is the wave vector of spin waves running transverse to the sample, and k_x is the wave vector along the sample. The parameter $n = 0,1$ characterizes the type of excitations. For $n = 1$ one obtains the spectrum of the traditional spin waves, whereas $n = 0$ leads to the spectrum of Winter (or flexural) wall modes which describe a curving of the Bloch wall. In the limit of an infinite sample the spin waves have an anisotropy gap $2a^3 K_e/s$, while the flexural modes are gapless. For the *finite* sample widths considered here, however, the transverse spin waves and in particular the flexural modes acquire an additional finite size gap. This gap arises since the first excitation in transverse direction involves the finite wave vector $k_{\min} = \pi/w$, where w denotes the maximal transverse dimension of the sample. As a consequence of these finite size gaps, all transverse excitations of type n around the Bloch wall get frozen out below a given temperature T for sample widths $w < w_n$, where w_n follows from Eq. (2.3):

$$w_n(T) = \pi \left[\frac{2A/(K_h + nK_e)}{\sqrt{1 + (\rho T)^2 - 4[nK_e/(K_h + nK_e)]} - 1}\right]^{1/2}. \qquad (2.4)$$

Here we have set $\rho = sk_B/(K_h + nK_e)a^3$. Note that w_n diverges when $k_B T$ approaches $n(2a^3/s)\sqrt{K_e(K_e + K_h)}$ (from above).

Since the minimal energy $\epsilon_{n=0,\mathbf{k}}$ of the flexural wall modes is always smaller than that of the spin wave modes (at the same wavevectors), *quasi-1D behavior at temperature T is established for sample widths $w < w_{n=0}(T)$.* For instance, we find $w_{n=0} = \pi\sqrt{A/K_h}$ at a "freezing" temperature $k_B T = 2\sqrt{2}K_h a^3/s$, where $K_h = 2\pi M_0^2$ for a slab as shown in Fig. 1. Typical numbers for Ni (see Table II) are $w_{n=0} \approx 250$ Å and $T \approx 1$ K. We note that these flexural wall modes are frozen out well above the typical crossover temperature T_c below which one expects to see quantum tunneling. This crossover temperature will be calculated below and is found to be of the order of 5 mK. For a given sample width w, the transverse spin waves ($n = 1$) with $k_x = 0, \mathbf{k}_\perp \neq 0$ are frozen out at even higher temperatures.

B. Soliton solutions and soliton mass

In the literature, various differing values for the wall mass have been used. Therefore we give now a derivation of the

wall mass from the *exact* soliton solutions[12] of the equations of motion (2.2). These soliton solutions describe Bloch walls traveling at a constant velocity v, and are given by[13]

$$\theta_0(x-vt)=2\arctan e^{(x-vt)/\tilde{\delta}}. \qquad (2.5)$$

The soliton velocity v is related to the (constant) azimuthal angle ϕ_0 by the expression

$$v=\sqrt{\frac{A}{K_e}}\frac{\gamma K_h}{M_0}\frac{\sin 2\phi_0}{\sqrt{1+\kappa\sin^2\phi_0}}, \qquad (2.6)$$

where

$$\kappa=K_h/K_e. \qquad (2.7)$$

We see that at finite velocities the magnetization is tilted out of the easy xz plane ($\phi_0=0,\pi$) and also that the Bloch wall has a limiting velocity (the "Walker limit")

$$v_w=v_0[\sqrt{1+\kappa}-1], \qquad (2.8)$$

where $v_0=2\gamma\sqrt{AK_e}/M_0$.

The width of the moving Bloch wall

$$\tilde{\delta}=\delta[1+\kappa\sin^2\phi_0]^{-1/2}, \qquad (2.9)$$

is contracted relative to the width $\delta=\sqrt{A/K_e}$ of a Bloch wall at rest. Inserting Eqs. (2.5) and (2.6) into (2.1) we obtain the total energy of a moving Bloch wall

$$E(\theta_0,\phi_0)=E_0\sqrt{1+\kappa\sin^2\phi_0}, \qquad (2.10)$$

where $E_0=4\mathcal{A}\sqrt{AK_e}$ is the energy of a static Bloch wall.

If the hard-axis anisotropy energy induced by the soliton motion is much smaller than the easy-axis anisotropy, i.e., $\kappa\sin^2\phi_0\ll 1$, then $v\ll v_0\sqrt{\kappa}$, and the energy in Eq. (2.10) takes the form

$$E(\theta_0,\phi_0)=E_0+\frac{M}{2}v^2, \qquad (2.11)$$

with the wall mass

$$M=\mathcal{A}\frac{M_0^2}{\gamma^2 K_h}\sqrt{\frac{K_e}{A}} \qquad (2.12)$$

(provided, of course, that $v<v_w$). For a hard axis of demagnetizing origin of the form $K_h=2\pi M_0^2$, Eq. (2.12) reduces to the Döring expression of the wall mass $M_D=(\mathcal{A}/2\pi\gamma^2)\sqrt{K_e/A}$.[14] We emphasize that in the presence of an additional strong crystalline hard-axis anisotropy, $K_h=2\pi M_0^2+K_{h,\mathrm{cryst}}$, with $K_{h,\mathrm{cryst}}\gg 2\pi M_0^2$, the wall mass (2.12) is substantially smaller than the Döring value (smaller masses lead to higher tunneling rates). Wall masses that are up to 10^3 smaller than the Döring value are found in the orthoferrites.[15]

Equation (2.11) shows that a moving domain wall behaves as a particle of mass M. The dynamics of the domain wall $\theta_0(x-X)$ with $X=X(t)$ can therefore be described by the action of a free particle of mass M

$$\mathcal{S}^{(0)}=\int dt\,\frac{M}{2}\dot{X}^2. \qquad (2.13)$$

For a microscopic derivation of Eq. (2.13) from the quantum spin action within a coherent spin state path integral formalism and a collective coordinate technique (and also including the effects of dissipation via spin waves) we refer the reader to Refs. 16,17,9.

C. Impurities and pinning potentials

So far we have focused on an ideal sample with perfect translational invariance. In realistic samples this invariance is broken by impurities or modulations of the sample cross section. We extend now the above considerations to this situation and discuss the effects of an external magnetic field. For simplicity we treat first a pointlike impurity, consisting of a single atom at $\mathbf{x}=0$ with easy-axis anisotropy $K_p\neq K_e$. Such an impurity can be described by changing the anisotropy constant in Eq. (2.1) in the following way:

$$K_e\rightarrow K_e+K_p(\mathbf{x}), \quad K_p(\mathbf{x})=-V_0\delta(\mathbf{x}), \qquad (2.14)$$

where $V_0=(K_e-K_p)a^3$, for ν such impurities we evidently have $V_0=\nu(K_e-K_p)a^3$. Without loss of generality, we consider in the sequel the case of attractive impurities, i.e., $V_0>0$.

A uniform external field along the $\hat{z}$ (easy) axis is described by a Zeeman term $-HM_0\cos\theta$ in the energy density (2.1). Both pinning and external field thus lead to the additional energy

$$E'=\int d^3x\{K_p(\mathbf{x})\sin^2\theta-HM_0\cos\theta\}. \qquad (2.15)$$

The impurity now breaks the translational symmetry transverse to the sample. We consider here the situation of weak pinning where the pinning energy is much smaller than the static wall energy $V_0/E_0\ll 1$. In this case deviations from the flat Bloch wall configuration (θ_0,ϕ_0) can be neglected. Note that $E_0=2NK_ea^3$, where $N=2\mathcal{A}\delta/a^3$ is the number of spins in the static wall. Therefore the weak pinning assumption can be satisfied even in the case of many impurities as long as the concentration of impurities within the wall volume is small.

To lowest order in V_0/E_0, we can then insert the static soliton solution $\theta_0(x-X)$ into Eq. (2.15) and obtain the additional energy[13]

$$E'=V_p(X)-hX, \qquad (2.16)$$

with the pinning potential

$$V_p(X)=-V_0\mathrm{sech}^2\left(\frac{X}{\delta}\right), \qquad (2.17)$$

and the force due to the external field

$$h=2\mathcal{A}M_0H. \qquad (2.18)$$

In Eq. (2.17) we have used that $\tilde{\delta}=\delta[1+O(v/v_0\sqrt{\kappa})^2]$. Note that even a pointlike pinning center of the form (2.14) creates a shallow potential (2.17) varying on the length scale of the Bloch wall width $\delta=\sqrt{A/K_e}$.

The pinning potential (2.17) not only holds for pointlike impurities but also describes pinning due to *variations in the cross section* if they extend over length scales l shorter than

the domain wall width δ. To be specific, let us consider a constriction where the cross sectional area $\mathcal{A}(x) = \mathcal{A} - \Delta\mathcal{A}(x)$ is locally reduced, i.e., $\Delta\mathcal{A}(x)$ vanishes for $|x| > l$. Let $\Delta v = \int dx \Delta\mathcal{A}(x)$ denote the missing sample volume of the constriction. The total wall energy is then

$$E' = \int dx \mathcal{A}(x)\{2K_e\sin^2\theta - HM_0\cos\theta\}$$

$$= -2K_e\Delta v \operatorname{sech}^2\frac{X}{\delta} - hX + \text{const}, \qquad (2.19)$$

where $\theta = \theta_0(x - X)$. Thus the effect of the constriction is again described by Eqs. (2.16), (2.17) but now with $V_0 = 2K_e\Delta v = E_0\Delta v/2\mathcal{A}\delta$. The weak-pinning limit is thus justified as long as the volume Δv is small compared to the volume $2\mathcal{A}\delta$ occupied by the domain wall. In the second line of Eq. (2.19), we have suppressed a small additional Zeeman term $(h\Delta v/2\mathcal{A})\tanh(X/\delta)$ which is an irrelevant constant for large X, while for small X it renormalizes h by a factor $1 - \Delta v/2\mathcal{A}\delta$. However, this renormalization is small in the weak pinning limit considered here and thus experimentally not relevant.

In conclusion, we find that the dynamics of a domain wall in an external field, and in the presence of a pointlike impurity (or a constricted cross section) is described by the action $\mathcal{S} = \mathcal{S}^{(0)} - \int dt E'$. Explicitly we have

$$\mathcal{S} = \int dt\left\{\frac{M}{2}\dot{X}^2 - V_p(X) + hX\right\}, \qquad (2.20)$$

with V_p as in Eq. (2.17). V_0 depends on the impurity or constriction parameters as defined above. The dynamics of the Bloch wall is thus seen to be equivalent to that of a particle of mass M in a potential V_p under a force h.

III. DEPINNING VIA QUANTUM TUNNELING

In this section we calculate the tunneling probability of a Bloch wall out of a pinning potential $V(X)$. For the moment, let us consider a pinning potential of arbitrary shape, as might arise, e.g., from the presence of many randomly located impurities. We shall return below to the specific case of the generic sech^2 potential.

Interested in tunneling phenomena, we consider the Euclidean version of the action (2.20)

$$\mathcal{S}_E = \int_0^\beta d\tau\left\{\frac{M}{2}\left(\frac{dX}{d\tau}\right)^2 + U(X)\right\}, \qquad (3.1)$$

where units have been chosen such that $\hbar = 1$. The potential energy for the wall is given by

$$U(X) = V(X) - hX. \qquad (3.2)$$

In Eq. (3.1), $\beta = 1/k_B T$, the wall mass M is given by Eq. (2.12), and $V(X)$ is some smooth pinning potential which, for the present, we keep arbitrary. It is only assumed that $V(X) < 0$ and that it tends to zero for $|X| \to \infty$. It then follows that $V(X)$ has at least two inflection points X_i, defined by $V''(X_i) = 0$.

Let us consider the situation of a vanishing external field where the wall is pinned at a local minimum $X_{\min}$ of $V(X)$.
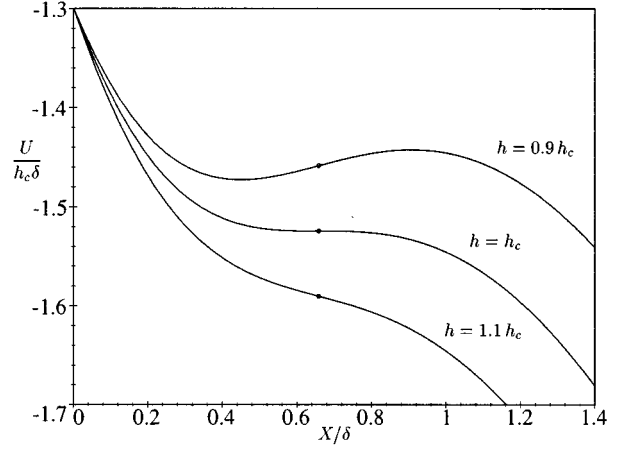

FIG. 2. We plot the potential energy $U(X)$ of Eq. (3.2) for the sech^2 pinning potential of Eq. (2.17). For this pinning potential, the coercivity h_c equals $(4/\sqrt{27})V_0/\delta$. The three curves show the potential energy for the external field h slightly above, right at, and slightly below the coercivity field h_c. By expanding about the inflection point (shown by small circles in the figure), these curves are very well approximated by a cubic potential, as discussed in the text.

Let X_i be the inflection point closest to the right of $X_{\min}$. Thus $V'(X_i) > 0$ and $V^{(3)}(X_i) < 0$. At small (positive) values of the external field, the wall is still trapped at $X_{\min}$, but as the field is increased, the potential becomes increasingly tilted and finally, the metastable state ceases to exist at the coercive force

$$h_c = V'(X_i), \qquad (3.3)$$

where $h_c = 2\mathcal{A}M_0H_c > 0$, with H_c the classical (zero temperature) coercivity. In Fig. 2 we plot the potential energy $U(X)$ with the sech^2 pinning potential of Eq. (2.17). The three curves shown are for external fields near the classical coercivity. It should be kept in mind, however, that the following analysis is valid for *arbitrary* pinning potentials (subject to the conditions expounded in the preceding paragraph).

The possibility of quantum tunneling arises when the external field is close to the classical coercivity, i.e.,

$$0 < \epsilon = 1 - H/H_c \ll 1. \qquad (3.4)$$

The potential (3.2) can then be expanded around the inflection point X_i of $U(X)$ to yield

$$U(x) = \frac{1}{6}V^{(3)}(X_i)x^3 + \left(-\frac{1}{2}\epsilon h_c V^{(3)}(X_i)\right)^{1/2}x^2$$

$$= \frac{27}{4}V_{\max}\left(\frac{x}{d}\right)^2\left(1 - \frac{x}{d}\right). \qquad (3.5)$$

Several comments are in order regarding these expressions. First, the third derivative $V^{(3)}(X_i) < 0$ in general depends on the coercivity. Also, we have shifted coordinates so that the minimum is now $U(0) = 0$. In the second line, we have introduced the tunneling distance $d > 0$, defined by $U(d) = 0$, and the barrier height $V_{\max}$. These are explicitly given by[18]

$$V_{\max} = \frac{2^{5/2}}{3} \frac{(h_c \epsilon)^{3/2}}{[-V^{(3)}(X_i)]^{1/2}}, \qquad (3.6)$$

$$d = 3\sqrt{2} \frac{(h_c \epsilon)^{1/2}}{[-V^{(3)}(X_i)]^{1/2}}. \qquad (3.7)$$

For external fields close to the coercivity, the Euclidean action associated with the tunneling of the domain wall is thus given by

$$\mathcal{S}_E[x] = \int_0^\beta d\tau \left\{ \frac{M}{2} \left(\frac{dx}{d\tau} \right)^2 + U(x) \right\}, \qquad (3.8)$$

with $U(x)$ as in Eq. (3.5). This action is rendered stationary by the ''bounce'' trajectory

$$x_b(\tau) = d\, \mathrm{sech}^2 \omega_b \tau \qquad (3.9)$$

which runs from $x=0$ to $x=d$ and *back* to $x=0$ for τ increasing from $-\beta/2$ to $\beta/2$ with $\beta \to \infty$. The characteristic tunnel frequency is given by

$$\omega_b = (3/2)^{3/2} \sqrt{V_{\max}/Md^2}. \qquad (3.10)$$

Note that ω_b is half the harmonic oscillation frequency in the potential minimum of U. The tunneling action $\mathcal{S}_0 = \mathcal{S}[x_b]$ can be calculated without explicit knowledge of the above bounce trajectory, i.e.,

$$\mathcal{S}_0 = 2\sqrt{2M} \int_0^d dx \sqrt{U(x)}, \qquad (3.11)$$

$$= 4\sqrt{\frac{6}{5}} d\sqrt{MV_{\max}} = \frac{18}{5} \frac{V_{\max}}{\omega_b}. \qquad (3.12)$$

Note that the factor of 2 in the first equation arises because the escape rate is determined by the action over the whole bounce which leads from $x=0$ to $x=d$ and back to $x=0$.

The escape tunneling rate P for the potential U in Eq. (3.2) has been calculated before in a different context [see, e.g., Weiss,[19] p. 109, Eqs. (8.12) and (8.16)]. It is explicitly given by the standard WKB expression

$$P = 4\omega_b \sqrt{15 \mathcal{S}_0 / 2\pi}\, e^{-\mathcal{S}_0}. \qquad (3.13)$$

Typically, quantum tunneling will be observable if the time between tunneling events, i.e., the inverse escape rate P^{-1}, does not exceed a few hours. For a typical attempt frequency ω_b (given approximately by the exponential prefactor in P) of the order of 10^9 s^{-1} this requires that the exponent $\mathcal{S}_0/\hbar$ be less than about 30.

For the observation of quantum tunneling it is also important to ensure that the thermally activated transition rate *over* the barrier $P_T = \omega_0 \exp[-V_{\max}/k_B T]$, does not exceed the tunneling rate P *through* the barrier. This is the case if the sample temperature T is less than the crossover temperature T_c, which can be estimated by equating the corresponding transition rates. By assuming that the prefactors are approximately equal we have (after reinstating $\hbar$) the relation $k_B T_c = V_{\max} \hbar / \mathcal{S}_0$, which yields

$$k_B T_c = \frac{5}{8d} \sqrt{\frac{2 V_{\max}}{3M}} = \frac{5}{18} \hbar \omega_b. \qquad (3.14)$$

In order to obtain further quantitative understanding, we now apply the above results to the specific case of the generic pinning potential $V_p(X) = -V_0 \mathrm{sech}^2(X/\delta)$. With Eqs. (3.3), (3.6), and (3.7) we immediately find that

$$h_c = \frac{4}{3^{3/2}} \frac{V_0}{\delta}, \quad V_{\max} = \frac{2\sqrt{2}}{3} h_c \delta \epsilon^{3/2}, \quad d = 3\delta \sqrt{\frac{\epsilon}{2}}. \qquad (3.15)$$

The coercive force is thus linked to intrinsic properties of the pinning potential—the ratio of potential strength V_0 and characteristic length scale δ. Comparison of these expressions with Eqs. (3.7) and (3.6) shows now explicitly that $V^{(3)}(X_i) = -4h_c/\delta^2$ indeed depends on the coercive force.

The tunneling exponent, crossover temperature, and tunneling frequency follow from Eqs. (3.12), (3.14), and (3.10) and are given by

$$\mathcal{S}_0 = (6/5)\hbar Ns \sqrt{H_c/2\pi M_0} (2\epsilon)^{5/4}, \qquad (3.16)$$

$$k_B T_c = (5/18) g\mu_B \sqrt{2\pi M_0 H_c} (2\epsilon)^{1/4}, \qquad (3.17)$$

$$\omega_b = (g\mu_B/\hbar) \sqrt{2\pi M_0 H_c} (2\epsilon)^{1/4}, \qquad (3.18)$$

TABLE I. Summary of equivalent expressions for bounce frequency ω_b, WKB exponent $\mathcal{S}_0/\hbar$, and crossover temperature T_c. $N = 2\delta \mathcal{A}/a^3$ denotes the number of spins in the wall. In the last column it has been assumed that $K_h = 2\pi M_0^2$, i.e., the sample has the slab geometry of Fig. 1 and there is no crystalline hard-axis anisotropy, $K_{h,\mathrm{cryst}} = 0$.

ω_b	$\left(\dfrac{3}{2}\right)^{3/2} \dfrac{1}{d} \sqrt{\dfrac{V_{\max}}{M}}$	$\sqrt{\dfrac{h_c}{M\delta}} \left(\dfrac{\epsilon}{2}\right)^{1/4}$	$\gamma \sqrt{\dfrac{2H_c K_h}{M_0}} \left(\dfrac{\epsilon}{2}\right)^{1/4}$	$2^{3/4} \dfrac{g\mu_B}{\hbar} \sqrt{H_c M_0 \pi}\, \epsilon^{1/4}$
$\mathcal{S}_0$	$\sqrt{\dfrac{3}{2}} \dfrac{8}{5} d\sqrt{MV_{\max}}$	$2^{3/4} \dfrac{12}{5} \sqrt{Mh_c}\, \delta^{3/2} \epsilon^{5/4}$	$2^{3/4} \dfrac{6}{5} \hbar Ns \sqrt{\dfrac{2H_c M_0}{K_h}} \epsilon^{5/4}$	$2^{3/4} \dfrac{6}{5} \hbar Ns \sqrt{\dfrac{H_c}{\pi M_0}} \epsilon^{5/4}$
T_c	$\sqrt{\dfrac{2}{3}} \dfrac{5}{8} \dfrac{\hbar}{k_B} \dfrac{1}{d} \sqrt{\dfrac{V_{\max}}{M}}$	$2^{3/4} \dfrac{5}{36} \dfrac{\hbar}{k_B} \sqrt{\dfrac{h_c}{M\delta}} \epsilon^{1/4}$	$\dfrac{5}{18} \dfrac{g\mu_B}{k_B} \sqrt{\dfrac{K_h H_c}{M_0}} (2\epsilon)^{1/4}$	$2^{3/4} \dfrac{5}{18} \dfrac{g\mu_B}{k_B} \sqrt{\pi H_c M_0}\, \epsilon^{1/4}$

TABLE II. Saturation magnetization M_0, shape anisotropy $K_h = 2\pi M_0^2$ for a thin film, easy-axis anisotropy constant K_e, exchange A, wall width $\delta = \sqrt{A/K_e}$, wall mass M, and coercivity H_c for various materials.

	M_0 [Oe]	K_h [10^5 erg /cm^3]	K_e [10^5 erg/cm^3]	A [10^{-6} erg/cm]	δ [Å]	M/area [10^{-10} g/cm^2]	H_c [Oe]
YIG	196 [a]	2.4	0.25 [b]	0.43 [a]	414	1.2	10
Ni	508 [c]	16	8 [d]	1	112	4.6	100
large K_e [e]	200	2.5	100	1	32	16	10
SrRuO$_3$ [f]	159	1.6	20	0.023	11	48	10^4

[a]Ref. 23, p. 65.
[b]Ref. 24, p. 313.
[c]Ref. 25, p. 270.
[d]Ref. 25, p. 569.
[e]Example given in Ref. 7, parameters taken from there except for A which has been replaced by the most common value.
[f]Ref. 20.

where $N = 2\mathcal{A}\delta/a^3$ is the total number of spins in the wall and we have assumed a purely shape-induced hard-axis anisotropy, i.e., $K_h = 2\pi M_0^2$ for a slab geometry. Alternative but equivalent expressions for the bounce frequency ω_b, the WKB exponent $\mathcal{S}_0/\hbar$, and the crossover temperature T_c are listed in Table I.

To illustrate the above analytical results with concrete numbers we have collected in Tables II and III various values for several ferromagnetic samples of the shape shown in Fig. 1, namely yttrium iron garnet (YIG), nickel, the perovskite SrRuO$_3$,[20,21] and ''large easy-axis'' materials considered in Ref. 7. From Table III it becomes clear that the typi-

cal number N of spins one can expect to tunnel coherently out of a pinning potential within reasonable time (a few hours or less) is of the order of 10^4 or less, and that the associated crossover temperature T_c is typically less than 10 mK. A stark exception to this is SrRuO$_3$, in which our theory predicts 10^3 spins can coherently tunnel approximately once every millisecond with a crossover temperature of 37 mK. It would therefore be very interesting to look for domain wall tunneling in this material.

From Eqs. (3.16)–(3.18) we see that in order to optimize the observability of quantum tunneling it would be desirable to have materials that possess both a large coercivity H_c and

TABLE III. Cross-sectional area $\mathcal{A}$, number of spins N in the wall, ϵ, tunneling distance d, crossover temperature T_c, WKB exponent $\mathcal{S}_0/\hbar$, oscillation frequency ω, and inverse tunneling rate P^{-1} for various materials.

	$\mathcal{A}$ [Å^2]	ϵ	d [Å]	T_c [mK]	$\mathcal{S}_0/\hbar$	ω [10^9 s^{-1}]	P^{-1} [s]
YIG	50×200	10^{-1}	280	3	1268	2.6	∞
	[$N = 3.4\times10^4$]	10^{-2}	88	1.6	71	1.5	2×10^{20}
		5.7×10^{-3}	66	1.4	31.1	1.3	1433
		10^{-4}	8.8	0.5	0.2	0.47	2×10^{-9}
Ni	50×200	10^{-1}	75	14	1740	13	∞
	[$N = 2.4\times10^4$]	10^{-2}	23	8	98	7.6	10^{31}
		3.9×10^{-3}	15	6.3	31.1	6	310
		10^{-4}	2.4	2.5	0.3	2.4	3×10^{-10}
large K_e	50×200	10^{-1}	21	3	98	2.6	5×10^{31}
	[$N = 8.0\times10^4$]	3.6×10^{-2}	13	2.1	31.1	2	931
		10^{-2}	7	1.6	5.5	1.5	2×10^{-8}
		10^{-4}	0.7	0.5	2×10^{-2}	0.47	5×10^{-9}
SrRuO$_3$	50×200	10^{-1}	7.4	79	873	37	∞
	[$N = 3.4\times10^3$]	10^{-2}	2.3	44	49	21	10^9
		5×10^{-3}	1.7	37	21	18	10^{-3}
		10^{-3}	0.74	25	2.8	12	10^{-10}

a large hard axis anisotropy K_h but with the ratio $H_c/\sqrt{K_h}$ being small. Such materials would have a small WKB exponent (i.e., a high tunneling rate) *and* a high crossover temperature. There is, however, some leeway by carefully choosing the experimentally tunable parameters N and ϵ (see, e.g., $SrRuO_3$ in Tables II and III).

IV. DISCUSSION

A. Comparison with earlier results

A discussion of domain walls tunneling out of impurity potentials has been given by Chudnovsky, Iglesias, and Stamp[7] which we shall henceforth refer to as CIS (for earlier work in this field see also the references contained in CIS). Our results presented in Table III for experimentally vital quantities such as the WKB exponent S_0 and the crossover temperature T_c to the quantum regime differ substantially from the results given in Sec. VII of CIS. Therefore a comparison of the two approaches appears necessary.

Before turning to the most crucial difference between the two approaches—the functional dependence of the pinning potential on the coercivity—let us first remark that the mass M^{CIS} used in CIS differs from the soliton mass M given in Eq. (2.12). In fact,

$$M^{CIS} = M \frac{\kappa}{(\sqrt{1+\kappa}-1)^2}. \qquad (4.1)$$

The two masses agree only in the limit of large hard-axis anisotropy, i.e., $\kappa \equiv K_h/K_e \gg 1$. However, in the experimentally important limit of $\kappa \ll 1$ we have $M^{CIS}/M = 4/\kappa \gg 1$. Thus, we would expect our action to be smaller and the crossover temperature larger than the CIS results.

However, this tendency is more than compensated by the CIS assumption that the pinning potential width $\bar{w}$ is independent of the coercivity. For a field close to the coercivity, CIS find [their Eq. (25)] for the total pinning potential of arbitrary shape

$$A_w U(Z) = \sigma_0 A_w \left\{ \frac{\sqrt{2h_c^{CIS}\epsilon}}{2\bar{w}} \left(\frac{Z}{\delta}\right)^2 - \frac{1}{6\bar{w}^2} \left(\frac{Z}{\delta}\right)^3 \right\}, \quad (4.2)$$

where $h_c^{CIS} = \delta h_c/E_0$, $\sigma_0 A_w = E_0$, and $A_w = \mathcal{A}$. $\bar{w}$ is a parameter which is assumed to be independent of h_c and is set equal to unity in Sec. VII of CIS. However, comparison with our Eq. (3.5) reveals that the parameter $\bar{w}^2 = -\sigma_0 A_w/V^{(3)}(X_i)\delta^3$ is not arbitrary but depends on the details of the pinning potential.

In particular, for the generic $sech^2$ pinning potential (2.17) it follows that $\bar{w}$ is coercivity dependent:

$$\bar{w} = \frac{1}{2\sqrt{h_c^{CIS}}}. \qquad (4.3)$$

Since experimentally $h_c^{CIS} = H_c/H_a$ (where $H_a = 2K_e/M_0$) lies typically in the range $10^{-2} - 10^{-5}$, this implies a value of $\bar{w}$ in the range 5–100.

By assuming $\bar{w} \simeq 1$ in their final section, CIS have thus *a priori* fixed the depth of the pinning potential to the ex-

tremely large value of a third of the total wall energy $V_0 = E_0/3$. This situation corresponds to a region of length $4\delta/3$ extending across the entire cross sectional area being replaced with magnetic ions of vanishing anisotropy.

If we insert our expressions for M and $\bar{w}$ into Eq. (27) of CIS, then their tunneling action agrees with ours [up to a minor error of a missing factor of $2^{1/4}$ in Eq. (27) of CIS]. With these substitutions we also find agreement between our T_c and Eq. (44) of CIS (where again a factor $2^{-1/4}$ is missing).

Our results strikingly differ from CIS when it comes to the explicit computation of experimentally important quantities. In Eqs. (88) and (87) of CIS, numerical factors $2^{1/4}48/5 \simeq 11$ and $5\sqrt{2}/2^{1/4}36 \simeq 1/6$ respectively are suppressed compared to CIS Eqs. (27) and (44) for S_0 and T_c. Together with their assumption that $\bar{w} \simeq 1$, this leads (for a material with $h_c^{CIS} = 10^{-3}$) to an underestimation of the WKB exponent S_0 by a factor of 700 for a planar domain wall tunneling through the potential of a single defect. At the same time the crossover temperature T_c between quantum tunneling and thermal depinning is overestimated by a factor of 24.

Finally, we mention that while our crossover temperatures and WKB exponents differ substantially from the values presented in CIS, we find the same scaling of T_c and S_0 with respect to the reduced field ϵ.

B. A mechanism for increasing T_c

Explicit expressions for various materials such as Ni, Fe, YIG, and $SrRuO_3$ are presented in Table III. It is seen that the transition temperatures are in the mK range. A notable exception is $SrRuO_3$, whose small domain wall width leads to a narrow potential well and thus to a considerably higher transition temperature—around 40 mK.

We must mention, however, that our simple analysis here does not rule out discernible tunneling of larger walls at higher temperatures. Recent experiments on domain wall dynamics[8] have been interpreted as evidence of tunneling. This evidence primarily stems from the occurrence of temperature independent phenomena below a crossover temperature of a few Kelvin—*three orders of magnitude larger than our estimates here*. Rather than comment on these experiments, we will instead discuss a plausible mechanism which may raise T_c and/or decrease S_0.

Table III shows that the tunneling rate becomes appreciable if the tunneling distance is smaller than 10 Å. Thus, variations of the pinning potential $V(X)$ on this length scale could dramatically affect the tunneling behavior. Such variations do not occur for a random superposition of pinning potentials of the $sech^2$ type. However, under certain circumstances the underlying crystal lattice can provide such a modulation, in particular if the wall width is only a few lattice constants.

To get some quantitative ideas about the consequences of a modulation with the period of the lattice constant, let us add the term $V_{per}(X) = V_1 \sin(2\pi X/a + \zeta)$ to the pinning potential in Eq. (3.2). Here, ζ is a phase which we conveniently choose as $\zeta = -2\pi X_i/a$, where X_i is the inflection point of the $sech^2$ potential, i.e., $sech^2 X_i/\delta = 2/3$. Thus X_i remains the inflection point of $V + V_{per}$. This new potential has asso-

ciated with it a coercivity which is a factor of $(1+\mu)$ larger than the coercivity in Eq. (3.15), i.e., $h_c = h_c^{\text{old}}(1+\mu)$, where

$$\mu = \frac{\sqrt{27}\pi}{2} \frac{V_1 \delta}{V_0 a}. \tag{4.4}$$

In the vicinity of X_i, we can carry out the same expansion as outlined above to again obtain the cubic potential given by

$$V(x) = \sqrt{2\epsilon} \frac{h_c}{\delta} \lambda x^2 - \frac{2h_c}{3\delta^2} \lambda^2 x^3. \tag{4.5}$$

The new parameter λ, which equals unity for $V_1 = 0$, is given by

$$\lambda = \left(\frac{1 + r^2 \mu}{1 + \mu} \right)^{1/2}, \tag{4.6}$$

where $r = \pi \delta / a$. In Eq. (4.5) we have also redefined the reduced field ϵ to reflect the increased coercivity, i.e.,

$$\epsilon = 1 - \frac{h}{h_c} = \frac{\epsilon^{\text{old}} + \mu}{1 + \mu}. \tag{4.7}$$

Note that we now remain in the tunneling regime (i.e., $\epsilon > 0$) even if ϵ^{old} becomes negative. Equation (4.5) gives rise to a new tunneling distance d and also a new barrier height V_{max}, which results in a larger crossover temperature T_c and a reduced WKB exponent $\mathcal{S}_0$. These new expressions are explicitly given by

$$T_c = T_c^{\text{old}} \sqrt{(1+\mu)\lambda}, \tag{4.8}$$

$$\mathcal{S}_0 = \mathcal{S}_0^{\text{old}} \sqrt{(1+\mu)/\lambda^3}, \tag{4.9}$$

where T_c^{old} and $\mathcal{S}_0^{\text{old}}$ contain the *new* definition of ϵ, Eq. (4.7), since it is now ϵ (and not ϵ^{old}) which is the experimentally tunable parameter controlling the barrier height for tunneling. To obtain a numerical estimate of this effect, we need to estimate the magnitude V_1 of the periodic piece relative to the impurity strength V_0. Let us take, for example, $V_1 = 10^{-1} V_0$ and a domain wall of ten lattice constants, $\delta = 10a$. In this case, $T_c \approx 10 T_c^{\text{old}}$ and $\mathcal{S}_0 \approx 10^{-2} \mathcal{S}_0^{\text{old}}$. The estimates here for the WKB exponent must be taken with caution because these are estimates for the tunneling through *only one* of the (periodic) barriers. Due to the shape of the impurity potential, one should expect that there are $\sim \delta/a$ such barriers to tunnel through before the wall is free. Assuming incoherent sequential tunneling, $\mathcal{S}_0$ will effectively increase by a factor of about 10 for the estimates just given, i.e., $\mathcal{S}_0^{\text{eff}} \approx 10 \mathcal{S}_0$. Nevertheless, this very simple argument shows that observation of tunneling of larger walls at higher temperatures is not necessarily ruled out.

The case of a periodic potential superimposed on the impurity potential is interesting from another perspective. For $\epsilon^{\text{old}} = 0$ (but $\epsilon > 0$), the soliton originally pinned at the impurity now sees an effectively flat periodic potential through which it may tunnel *coherently*. Since the soliton is a particlelike excitation, we basically have here the physics of a particle in a periodic potential, and thus the soliton can form Bloch-like states of definite momentum.[9] Increasing the field still further induces a force on the soliton and the possibility

arises of Bloch oscillations *of a magnetic soliton.* This idea was first laid out semiclassically in Ref. 16 and essentially the same physics holds down to the extreme quantum case of spin-1/2.[22]

Finally, we briefly mention that thermally assisted tunneling may also raise the effective T_c. If the pinning potential contains some internal level structure, then the wall may be thermally excited to some higher level, and only then tunnel out of the pinning site. A more detailed analysis of this problem (e.g., along the lines discussed in the context of macroscopic quantum tunneling in superconducting quantum interference devices, see Weiss[19]) is required, however, before concrete statements concerning T_c can be made.

V. CONCLUSIONS

We have given in this paper a detailed derivation of the tunneling problem of a planar Bloch wall out of a pinning potential. We have focused exclusively on a quasi-one-dimensional ferromagnet with biaxial anisotropy, and have given estimates on when a system can be considered quasi-one dimensional. In particular, the flexural spin-wave modes, while gapless in infinite systems, acquire a gap for the finite geometries shown in Fig. 1. If the sample temperature is below this energy gap, then the flexural modes cannot be excited and can hence be neglected. For cross-sectional areas on the order of 10^4 Å^2, this energy gap is much larger than the crossover temperature at which quantum and thermal transitions are equal.

We have modeled the pinning center as an impurity which decreases the easy-axis anisotropy at a single point in space. Even such a pointlike impurity produces a shallow pinning potential which varies on the length scale of the Bloch wall width. We have related both the height and width of this potential to a coercivity. Detectable tunneling can only occur if the external field is very close to this coercivity, i.e., we must have $\epsilon = 1 - H/H_c$ on the order of 10^{-2} or 10^{-3}. This is an important number to determine experimentally. For example, if an experiment has $\epsilon \lesssim 0$, then one would also observe temperature independent depinning, but of course this cannot be ascribed to quantum tunneling—it is trivially due to the vanishing of the barrier height.

Within an instanton approach, the WKB exponent, bounce frequency, tunneling rate, and crossover temperature have been calculated and different analytical forms for these quantities can be found in Table I. We have also given estimates of these quantities for specific materials. The material parameters can be found in Table II, and the estimates in Table III. In particular, the perovskite $SrRuO_3$ seems a promising candidate and we hope this work can motivate some experimental studies into this material.

We have compared our results with previous work[7] and have found our calculations to predict lower crossover temperatures and a lower maximum number of spins which can coherently tunnel out of a pinning potential. Finally, we have briefly discussed how the effects of a periodic potential, may lead to a larger crossover temperature and a smaller WKB exponent.

[1] A. J. Leggett, *Quantum Tunneling in Condensed Media* (North-Holland, Amsterdam, 1992).

[2] *Quantum Tunneling in Magnetism*, Vol. 301 of *NATO Advanced Study Institute, Series E: Applied Sciences*, edited by B. Barbara and L. Gunther (Kluwer Academic, Dordrecht, 1995).

[3] T. Egami, Phys. Status Solidi A **20**, 157 (1973).

[4] T. Egami, Phys. Status Solidi B **57**, 211 (1973).

[5] B. Barbara *et al.*, Solid State Commun. **10**, 1149 (1972).

[6] P. C. E. Stamp, Phys. Rev. Lett. **66**, 2802 (1991).

[7] E. M. Chudnovsky, O. Iglesias, and P. C. E. Stamp, Phys. Rev. B **46**, 5392 (1992).

[8] K. Hong and N. Giordano, J. Phys.: Condens. Matter **8**, L301 (1996); in *Quantum Tunneling in Magnetism* (Ref. 2).

[9] H.-B. Braun and D. Loss, Phys. Rev. B **53**, 3237 (1996).

[10] We note that for a wire with *circular* cross section, one finds $K_e = K_{e,\text{cryst}}$ and $K_h = K_{h,\text{cryst}} + \pi M_0^2$, i.e., the shape-induced contribution to the hard axis anisotropy is half the value obtained for the slab geometry in Fig. 1.

[11] J. M. Winter, Phys. Rev. **124**, 452 (1962).

[12] L. Walker (unpublished), quoted in J. F. Dillon, in *Magnetism*, edited by G. R. Rado and H. Suhl (Academic, New York, 1963), Vol. III, pp. 450–453. For a review of theory and experiments on solitons in 1D magnetic systems see H.-J. Mikeska and M. Steiner, Adv. Phys. **40**, 191 (1991).

[13] Here we have fixed boundary conditions to $Q = \frac{1}{2}[\cos\theta(-\infty) - \cos\theta(+\infty)] = 1$. Equation (2.2) also admits solutions with $Q = -1$ which are obtained from Eq. (2.5) by the parity transformation $x \to -x$. The coupling to an external field along the $\hat{z}$ axis in Eq. (2.16) is then generalized to $-hQX$, thus characterizing Q as the (topological) ''magnetic charge'' of the soliton.

[14] W. Döring, Z. Naturforsch. **3A**, 373 (1948).

[15] A. P. Malozemoff and J. C. Slonczewski, *Magnetic Domain Walls in Bubble Materials* (Academic, New York, 1979).

[16] H.-B. Braun and D. Loss, J. Appl. Phys. **76**, 6177 (1994).

[17] H.-B. Braun and D. Loss, in *Quantum Tunneling in Magnetism* (Ref. 2).

[18] It is interesting to note that the ratio $V_{\max}/d = 4h_c\epsilon/9$ only depends on the coercivity and is otherwise independent of the details of the pinning potential $V(X)$.

[19] U. Weiss, *Quantum Dissipative Systems* (World Scientific, Singapore, 1993).

[20] L. Klein *et al.*, Appl. Phys. Lett. **66**, 2427 (1995).

[21] L. Klein (unpublished); (private communication).

[22] J. Kyriakidis and D. Loss (unpublished).

[23] T. H. O'Dell, *Ferromagnetodynamics* (Macmillan, London, 1981).

[24] R. S. Tebble and D. J. Craik, *Magnetic Materials* (Wiley-Interscience, New York, 1969).

[25] R. M. Bozorth, *Ferromagnetism* (Van Nostrand, New York, 1951).